Coherent interference of molecular electronic states in NO by two-color femtosecond laser pulses

Wenhui Hu,[1] Yong Liu,[2] Sizuo Luo,[1,*] Xing Li,[1] Jiaqi Yu,[1] Xiaokai Li,[1] Zhigang Sun,[2] Kai-Jun Yuan,[1,3,†]
André D. Bandrauk,[3] and Dajun Ding[1,‡]

[1]*Institute of Atomic and Molecular Physics, Jilin University, Changchun 130012, China*
[2]*State Key Laboratory of Molecular Reaction Dynamics, Dalian Institute of Chemical Physics,*
Chinese Academy of Sciences, Dalian 116023, China
[3]*Laboratoire de Chimie Théorique, Faculté des Sciences, Université de Sherbrooke, Sherbrooke, Québec, Canada J1K 2R1*

Quantum coherence interference between electronic states in molecules is an important factor for controlling electronic and nuclear dynamics in photoinduced physics and chemistry. We measure and model molecular angle-dependent photoionization yields to explore coherent interference dynamics between quasiequal energy electronic-vibrational states of the nitric oxide molecule, NO, by ultrafast phase-controlled two-color femtosecond laser pulses. We demonstrate by experiment and theory that the photoelectron angular distribution of NO, where two excited electronic states are coherently combined by ultrafast pulses, is a function of the relative phase of the pulses, and the photoelectron kinetic energy. The modification of photoelectron emission angular patterns encodes the information of the coherence via electronic state interference. The result allows access to phase-dependent state correlations and ultrafast vibrationic dynamics in molecules.

Imaging and controlling electronic and nuclear dynamics of molecules by ultrafast laser pulses is of great interest in the fields of photochemistry and photobiology [1–4]. The pump-probe technique of projecting an initial electronic-vibrational and rotational state onto accessible excited states is developing into a new ultrafast spectroscopy tool. Recent developments of ultrafast laser technology have led to photoimaging techniques such as Coulomb explosions for nuclear motion on a femtosecond (1 fs $= 10^{-15}$ s) timescale [5,6], to laser-induced electron diffraction (LIED) for coupled electron-nuclear motion on an attosecond (1 as $= 10^{-18}$ s) timescale [7–10]. Photoelectrons have a great potential for probing time-resolved transient structures of matter via ultrafast spectroscopy due to ultrashort electron timescales [11]. One now can explore electronic quantum effects through laser-induced electron interference and diffraction in materials and biology from femtosecond to attosecond regimes [12–16].

Laser-induced electronic state combinations with resulting wave-function superpositions can enhance ionization and induce transient localization of electron wave packets [17], thus allowing one to control the electron dynamics. Exploring electron-vibrational coherence requires highly spatiotemporal resolutions and remains a challenge in ultrafast science. Early studies on the laser control of photofragment angular distributions in molecular physics emphasized the importance of laser phase variations [18]. The nitric oxide molecule, NO, is adopted as a benchmark molecular system in chemical physics due to the presence of a single-electron occupied valence orbital [19,20]. Numerous phenomena in photoinduced molecular excitation and ionization processes of NO have been studied experimentally and theoretically in the past, e.g., Refs. [21–26]. By using general femtosecond pump-probe spectroscopy, interstate coherence and couplings have been studied [24,25]. It is found that time-resolved photoelectron spectra are generally modulated by intermediate Rydberg-valence state couplings and their dynamic Stark shift [26], thus suppressing the efficiency of the photoimaging. In this Rapid Communication, we present an experimental method using photoelectron imaging of coherent electronic-vibrational state interference in a diatomic molecule by two-color phase-controlled femtosecond laser pulses, and measure phase-controlled molecular photoelectron angular distributions of nonoriented NO to explore the laser-induced electronic-vibrational coherence dynamics. The control pulse modifies the excitation ionization as a function of the relative phase. By generating asymmetric electric fields via the temporal overlap between a fundamental frequency laser and its multiples, phase-controlled pulses lead to asymmetric photoelectron angular distributions which are shown to be dependent on the photoelectron kinetic energy and the relative phase of the pulses. Analysis by quantum theoretical and numerical modeling demonstrates that the dependence of photoelectron angular distributions on the photoelectron kinetic energy and the relative phase arises from the interference of two ionization channels, illustrating that different electronic states are entangled strongly within the molecules during ionization. This work thus provides a way to obtain information on the electron-vibration coherence dynamics of electronic states and effects on molecular excitations.

In the experiment, we extend the established resonance-enhanced multiphoton ionization (REMPI) technique to ultrafast phase-controlled photoelectron spectroscopy which is

---
*luosz@jlu.edu.cn
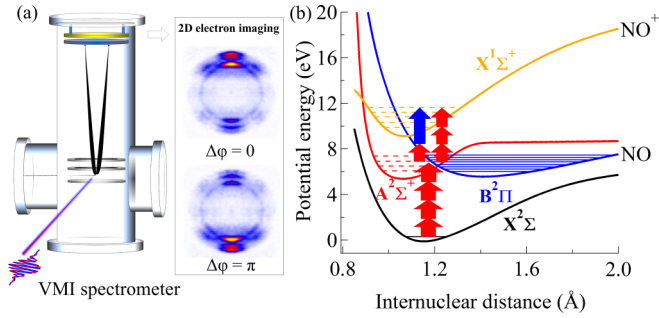†kaijun.yuan@usherbrooke.ca
‡dajund@jlu.edu.cn

FIG. 1. (a) Experimental setup for producing and measuring photoelectron momentum spectra by two-color phase-controlled laser pulses. Asymmetric photoelectron momentum at the relative phases $\Delta\varphi = 0$ and π are illustrated on the right. (b) Molecular potential energy curves. The arrows indicate the excitation and ionization pathways by the two-color femtosecond pulses: [red arrows (light gray in the grayscale version)] 4ω $X\,^2\Pi$-$A\,^2\Sigma^+$ and $X\,^2\Pi$-$B\,^2\Pi$ excitations in the molecule NO; 3ω [red (light gray) arrows] and $\omega + 2\omega$ [red +blue arrows (light gray + black gray in the grayscale version)] photoionization processes from the coherent state $\psi_c(\boldsymbol{R}, t)$ of NO to the ionic state $X\,^1\Sigma^+$ of NO$^+$.

briefly described below. As illustrated in Fig. 1(a), the apparatus consists of a chirped-pulse amplified (CPA) Ti:sapphire laser system, a stable phase-controlled two-color laser field generator, and a velocity map imaging spectrometer (VMIs) [27,28]. The fundamental frequency (ω) linearly polarized laser beam with 800-nm wavelength, 50-fs duration, 4 mJ per pulse energy, and 1-kHz repetition rate from the Ti:sapphire laser system is introduced into a β-BBO crystal to obtain its double-frequency 400-nm (2ω) pulse. Then the $\omega + 2\omega$ beam passes through a calcite to compensate the time delay caused by the group velocity delay of 800- and 400-nm laser beams in the whole optical path. The relative phase between the two-color lasers is accurately controlled by using a pair of fused silica wedges. A $\lambda/2$ plate for 800 nm is used to rotate the polarization of the fundamental frequency (ω) beam collinearly with that of double frequency (2ω), and a dual $\lambda/2$ plate is used to rotate the polarization of all laser fields to the same direction parallel with the detector plane. This phase-controlled laser beam is focused by a concave mirror ($f = 30$ cm) into the VMIs and interacts with a supersonic molecular beam of 1% NO seeded in neon. The generated electrons are projected onto a microchannel plate (MCP)-phosphor screen assembly. The images are recorded with a CCD camera, and finally transferred into a computer for data processing.

The two-color linearly polarized optical field can be given by

$$E(t) = E_\omega f(t)\cos(\omega t) + E_{2\omega} f(t)\cos(2\omega t + \Delta\varphi), \quad (1)$$

where $E_{\omega/2\omega}$ is the amplitude of the electric field and $f(t)$ denotes the common pulse envelope. Frequencies ω and 2ω correspond to wavelengths 800 and 400 nm, and $\Delta\varphi$ is the relative phase of the two laser pulses. The ω pulse intensity is adjusted by a neutral density filter, the relative intensity between ω and 2ω pulses is changed by rotating the phase-matching angle of the β-BBO crystal as required, and the intensity ratio $I_{2\omega}/I_\omega$ of the two-color laser field is about

0.08. We experimentally measured the electron images under different relative phases between 800- and 400-nm lasers in steps of 0.08π, and for avoiding smearing out the asymmetry properties, the iterative Abel inversion method [29] has been used to reconstruct the three-dimensional (3D) slice and extract the energy spectra and angular distributions.

We first prepare a coherent excited state with a $\lambda = 800$ nm laser pulse at an intensity of $I_\omega = 1.1 \times 10^{13}$ W/cm^2. Such low intensity avoids inner-shell ionization [30]. The molecule NO, initially prepared in its ground electronic state $X\,^2\Pi$ obtained from the cold molecular beam, is excited by the absorption of four ω photons to a coherent superposition of the $A\,^2\Sigma^+$ (A) and $B\,^2\Pi$ (B) electronic states, as illustrated in Fig. 1(b). The nonoriented molecule allows both parallel and perpendicular transitions by laser pulses. Moreover, the photoionization asymmetry due to molecular geometry asymmetry disappears. The two $A\,^2\Sigma^+$ and $B\,^2\Pi$ states are coupled weakly by negligible nonadiabatic rotational coupling with a crossing of their electronic potentials at $R \cong 1.2$ Å corresponding to equilibrium of the ground state [31]. The corresponding wave function $\psi_c(\boldsymbol{R}, t)$ of the excited nuclear coherent-state combination is [32]

$$\psi_c(\boldsymbol{R}, t) = \psi_A(\boldsymbol{R}, t) + \psi_B(\boldsymbol{R}, t), \quad (2)$$

where $\psi_A(\boldsymbol{R}, t) = \sum_{vjm} c_{vjm}(t)\psi_v(R)\psi_{jm}(\theta, \phi)e^{-iE_{vjm}t/\hbar}$ is for the $A\,^2\Sigma^+$ state and $\psi_B(\boldsymbol{R}, t) = \sum_{v'j'm'} c_{v'j'm'}(t)\psi_{v'}(R)\psi_{j'm'}(\theta, \phi)e^{-iE_{v'j'm'}t/\hbar}$ is for the $B\,^2\Pi$ state, and $\psi_{v/v'}(R)$ and $\psi_{jm/j'm'}(\theta, \phi)$ are the wave functions of the vibrational v/v' and rotational $jm/j'm'$ stationary states with total eigenenergies $E_{vjm/v'j'm'}$, respectively. $c_{vjm}(t)$ and $c_{v'j'm'}(t)$ are the occupation coefficients determined by the intensity of the driving laser pulse. The two-state $A\,^2\Sigma^+$–$B\,^2\Pi$ coherence describes the ultrafast excitation and charge transfer of molecules under the laser interaction. In order to study the coherence of the two electronic states, we introduce a control $\lambda = 400$ nm ($2\hbar\omega = 3.1$ eV, $I_{2\omega} = 8.9 \times 10^{11}$ W/cm^2) weaker pulse with the same $f(t)$ and measure the corresponding phase-controlled photoelectron spectra versus the phase difference $\Delta\varphi$ in Eq. (1). The ionization of the excited molecule can thus be coherently controlled by varying the relative phase between the $\lambda = 400$ nm and the $\lambda = 800$ nm pulses. The weaker 400-nm pulse does not influence significantly the molecular coherent excitation between the ground $X\,^2\Pi$ and the excited $A\,^2\Sigma^+$ and $B\,^2\Pi$ electronic states. Furthermore, in the phase-controlled photoelectron spectra, the effect of interstate nonadiabatic coupling and the intermediate higher Rydberg excited electronic states on the exploration of the coherent coupling are negligible.

Figure 2(a) presents the photoelectron momentum spectrum produced by the two-color femtosecond laser pulses as illustrated in Fig. 1(b), which is obtained by averaging the results over the relative phase $\Delta\varphi$ from -2π to 2π. At such high intensities, the asymmetry of photoelectron angular distributions resulting from the molecular orientational asymmetry disappears [33]. It is found that the photoelectron spectra exhibit multiple angular nodes (angles I and II) with respect to the laser polarization direction and four separated peaks at energies 0.29, 0.67, 0.97, and 1.25 eV, marked as 1–4
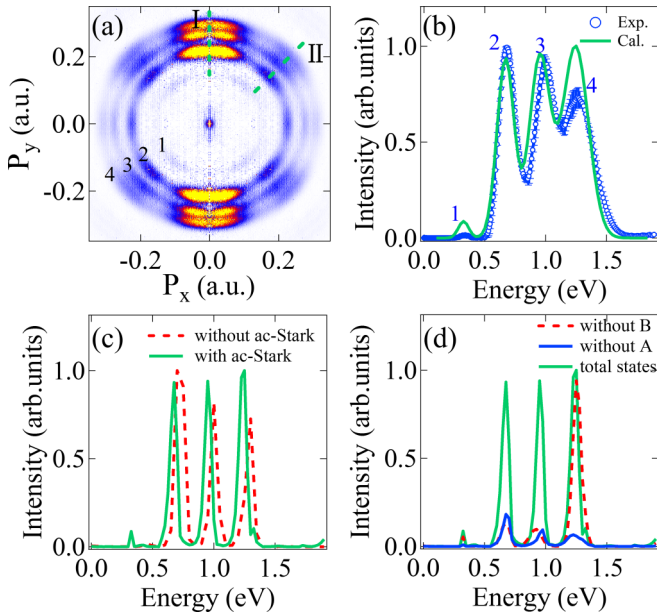
FIG. 2. Photoionization yields of the molecule NO by a two-color laser field. (a) Averaged two-dimensional (2D) photoelectron momentum distributions over the relative phases $\Delta\varphi$ varying from -2π to 2π. Angles I and II at 0° and 45° denote photoelectron emission directions with respect to the laser polarization. (b) The corresponding photoelectron energy spectra by integrating over the angle from the experiment (the blue circle) and the simulation result with the instrument response (the green solid line). The separate peaks illustrate the molecular vibrational levels of the intermediate electronic states. (c) and (d) Simulation results from numerical solutions of TDSEs. To illustrate the effect of coherent-state combinations, the results from the excitation processes of the single resonant intermediate A ($A\,^2\Sigma^+$) or B ($B\,^2\Pi$) electronic state are also presented in (d) for comparison.

in Fig. 2. The experimental photoelectron energy spectrum and the simulation spectrum with the instrument response are displayed in Fig. 2(b). With the laser field at 800 nm dominating, as shown in Fig. 1(b), four ω photons are required from the ground state in resonance with the excited intermediate $A\,^2\Sigma^+$ and $B\,^2\Pi$ electronic states at $\Delta E = 6.2$ eV $= 4\hbar\omega$, that is, producing the coherent state $\psi_c(\mathbf{R}, t)$, as expressed in Eq. (2). Simultaneously, REMPI occurs from the coherent superposition of electronic state $\psi_c(\mathbf{R}, t)$, to the ionic state $X\,^1\Sigma^+$ of NO^+, giving rise to the photoelectron spectra. The angular distributions reflect the ionization symmetry and the separated energy peaks identify the vibrational levels of the coherent electronic states [34,35]. Two pathway ionization processes after absorption of three photons (3ω) or two photons ($\omega + 2\omega$) from the coherent state, $\psi_c(\mathbf{R}, t)$, as illustrated in Fig. 1(b), interfere with each other, leading to asymmetric angular distributions which are functions of the relative phase $\Delta\varphi$ of the pulses and of photoelectron kinetic energy.

To interpret the experimental results, we performed quantum simulations to obtain solutions of the time-dependent Schrödinger equations (TDSEs) of the molecule NO within the Born-Oppenheimer approximation, in the presence of the laser pulse, Eq. (1),

$$i\hbar\frac{\partial}{\partial t}\psi(R, \theta, t) = \left[-\frac{\hbar^2}{2m_d}\frac{\partial^2}{\partial R^2} + \frac{J^2}{2m_d} + V(R) + V_L(R, \theta, t)\right]\psi(R, \theta, t), \quad (3)$$

where R is the molecular internuclear distance and θ is the angle between the electric field and the molecular axis. m_d is the reduced mass and $V(R)$ are molecular potentials, as in Fig. 1(b). $V_L(R, \theta, t)$ is the field-molecule interaction term,

$$V_L(R, \theta, t) = \begin{cases} -\mu_{ij}(R)E(t)\cos(\theta) & \Delta\Lambda = 0, \\ -\mu_{ij}(R)E(t)\sin(\theta) & \Delta\Lambda = \pm 1, \end{cases} \quad (4)$$

where $\Delta\Lambda = 0$ and ± 1 present parallel (such as $X\,^2\Pi$-$B\,^2\Pi$) and perpendicular (such as $X\,^2\Pi$-$A\,^2\Sigma^+$) transitions between the i and j electronic states, and μ_{ij} is the corresponding electronic transition dipole moment [31]. A Gaussian envelope $f(t)$ is chosen for the electric field $E(t)$ in Eq. (1). The TDSE in Eq. (3) is numerically solved with a sine-Legendre discrete variable representation [36] in combination with second-order split operation propagation technique [37]. The photoelectron spectra are obtained by calculating numerically the photoionization probability in the electron continuum state, $X\,^1\Sigma^+$ of the cation NO^+. The ionization continuum is discretized into a band of quasicontinuum levels in terms of the electron eigenstates $|\varepsilon\rangle$ for the $X\,^1\Sigma^+$ nuclei and electrons [36,37]. The continuum states are labeled according to the kinetic energy ε of the ejected electrons $|\psi_I(R, t)\rangle = \int d\varepsilon\psi_{X'}(R, \varepsilon, t)|\varepsilon\rangle$, where $\psi_{X'}(R, \varepsilon, t)$ are the vibrational wave functions of NO^+. Moreover, the ponderomotive energy of electronic states in the electric field $E_\omega(t)$, $U_p = e^2 E_\omega^2 / 4m_e\omega^2$, is taken into account exactly in the numerical solutions to describe the electron coherence. The observed kinetic energy of the photoelectron is represented as

$$\varepsilon_k = q\hbar\omega - (I_p - E_{A/B}) - (1 - \gamma)U_p, \quad (5)$$

where q is the photon number of absorption for ionization from the coherent electronic state $\psi_c(\mathbf{R}, t)$ and U_p is the ponderomotive energy corresponding to a maximum Stark shift of a free electron in an oscillating electric field [21,38]. γ is the ratio of the ac Stark shift of the Rydberg resonant states to the ponderomotive energy U_p [39] and is set at $\gamma = 0.85$. It should be noted that the ponderomotive energy is $U_p = 0.65$ eV for the 800-nm pulse at 1.1×10^{13} W/cm^2, whereas that resulting from the 400-nm pulse is very weak, 0.013 eV, and negligible in the ionization process. Therefore, the ac Stark shift is mainly induced by the 800-nm pulse due to its lower laser frequency and higher intensity. In Fig. 2, there is good quantitative agreement between the experimental and computational photoelectron spectra. Calculations show that the four separated photoelectron energy peaks are created respectively from the vibrational levels $v = 0$–3 of the $A\,^2\Sigma^+$ state and $v' = 4$–7 of the $B\,^2\Pi$ electronic state. The resonant excitation process from the ground $X\,^2\Pi$ state to the excited $A\,^2\Sigma^+$ and $B\,^2\Pi$ electronic states by the 800-nm pulse is dominant. The transition population induced by the 400-nm pulse is much weaker than that by the 800-nm pulse, about 1/10. Therefore, the multiple channel excita-

tion effects are negligible caused by the 800- and 400-nm pulses together or the 400-nm pulse solely. This confirms our experimental prediction (interpretation) that the coherent superposition $\psi_c(\boldsymbol{R}, t)$ in Eq. (2) mainly results from a four-ω resonant excitation process. As shown in Fig. 2(c), the ac Stark effect leads to a slight redshift of the photoelectron energy spectra, about 0.09 eV. As the energy of photoelectron increases, the ionization from the higher vibrational levels increases. We also compare the calculated results obtained from a single intermediate resonant $A\,{}^2\Sigma^+$ and $B\,{}^2\Pi$ electronic states. The corresponding photoelectron energy spectra are plotted in Fig. 2(d). From our simulations, it is found that there is a strong interference between the $A\,{}^2\Sigma^+$ and $B\,{}^2\Pi$ states from the four 800-nm photon ground-state excitations, which enhances the further ionization and results in an increase of the photoelectron spectra in amplitude, as described in the photoionization model [40].

In order to explore the coherent dynamics of the total electronic state ψ_c in Eq. (2), we measure the photoelectron spectra as functions of the emission angle θ and kinetic energy ε_k of photoelectrons, and the relative phase $\Delta\varphi$ of the pulses defined in Eq. (1). In the REMPI process, general time-resolved photoelectron spectra contain the information of intermediate resonant states. The evolution of the wave packets in these resonant states modulates the probing spectra. We here measure phase-controlled photoelectron emission spectra by the two-color femtosecond laser pulses, as shown in Fig. 1(b). In the phase-controlled photoelectron spectra, the effects of Rydberg states on the phase dependence are negligible, thus allowing one to reveal the net coherence of the electronic state ψ_c. Three cases at different photoelectron kinetic energies, i.e., peaks 2, 3, and 4, marked in Fig. 2(a), are compared. Figure 3 shows the evolution of photoelectron angular distribution spectra with the relative phase difference $\Delta\varphi$ and the photoelectron kinetic energies ε_k. Asymmetric angular distributions are produced in spite of the nonorientation of NO. Varying the phase $\Delta\varphi$ gives rise to a periodical oscillation with a period 2π. Of interest is that there is an energy dependence of photoelectron spectra on the relative phase $\Delta\varphi$. This reflects the multiple pathway ionization interference and the coherence of the electronic state ψ_c.

To clearly visualize the coherence effects, we show the phase dependence of photoelectron energy spectra at the ionization angles $0° \pm 20°$ (angle I) and $45° \pm 15°$ (angle II) in Figs. 3(d) and 3(e). The angular distributions reflect the shape of the ionizing orbitals [41]. For the $A\,{}^2\Sigma^+ \, \pi\sigma^*$ configuration and $B\,{}^2\Pi\, \pi^3\pi^{*2}$ configuration, the maxima of the photoelectron angular distributions appear at $0°$ (I) and $45°$ (II), corresponding to the σ and π^* orbital symmetries [42]. The periodical oscillation for the three cases at different angles corresponds to the interference effects between the two pathway ionization processes, which is also dependent on the photoelectron kinetic energy. As shown in Fig. 2(d) for peak 1, the photoelectron energy spectral intensity is very weak. We therefore focus on the three higher-energy spectrum peaks 2–4 with a strong coherent orbital combination. As illustrated in Fig. 3(f), for the angle I at $0° \pm 20°$, the maximum value of the spectral peak 2 occurs at $\Delta\varphi = 0.06\pi$. As the photoelectron kinetic energy increases, there is a shift of the maximum value to a smaller phase. For peak 4, the maximum lies at $\Delta\varphi = -0.16\pi$. Similar phenomena are also produced at the angle II at $45° \pm 15°$. The modifications of interference effects in the photoelectron spectra in Fig. 3 essentially illustrate the dynamics of the coherent-state combination of the intermediate resonant electron-vibrational states in molecular photoionization, which is described theoretically next.

The ionization from the coherent state $\psi_c(\boldsymbol{R}, t)$, created by the two-color ω and 2ω laser pulses, corresponds to an interfering three-photon (3ω) and two-photon ($\omega + 2\omega$) ionization process, as depicted in Fig. 1(b). For the photoelectron angular distributions at kinetic energy ε_k, the total transition probability is the square of the two amplitudes, $P_{3\omega}(\varepsilon_k)$ and $P_{2\omega+\omega}(\varepsilon_k)$, with an interference term via the cross products of the three- and two-photon ionization amplitudes, $P_{\mathrm{int}}(\varepsilon_k)$. The interference term can be simply written as [43–45]

$$
\begin{aligned}
P_{\mathrm{int}}(\varepsilon_k, t) = E_\omega^4 E_{2\omega} f^5(t) \big[&\big(T_3^A T_2^A + T_3^B T_2^B\big) \cos(\theta - \Delta\varphi) \\
&+ T_3^A T_2^B \cos(\Delta\varepsilon_k t/\hbar + \theta - \Delta\varphi) \\
&+ T_3^B T_2^A \cos(\Delta\varepsilon_k t/\hbar - \theta + \Delta\varphi) \big],
\end{aligned}
\tag{6}
$$

where $T_3^{A/B}$ and $T_2^{A/B}$ are the transition-matrix elements of the three- and two-photon ionization processes from respectively the $A\,{}^2\Sigma^+$ (A) and $B\,{}^2\Pi$ (B) electronic states, θ is the emission angle of the photoelectron with respect to the laser polarization direction, and $\Delta\varepsilon_k = \varepsilon_k - E_{vjm/v'j'm'}$. As shown in Fig. 2(d), the amplitudes of photoelectron spectra from the $A\,{}^2\Sigma^+$ (A) and $B\,{}^2\Pi$ (B) states are comparable, giving rise to the maximum interference effect. It is also found that the transition-matrix elements $T_3^{A/B}$ and $T_2^{A/B}$ are functions of the two electronic states $\psi_{A/B}$ [40]. The interference model in Eq. (6) thus encodes the information of the time-dependent coherent superposition state $\psi_c(t)$ in Eq. (2). Assuming the same transition-matrix elements for multiphoton ionization, we then can rewrite Eq. (6) by integrating over time t for a
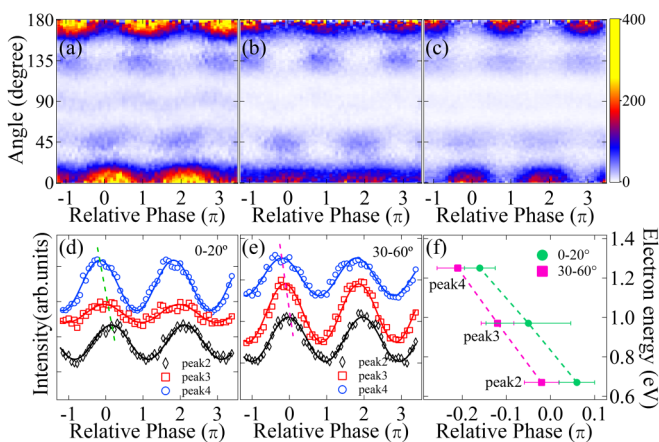

FIG. 3. Dependence of photoelectron spectra on the relative phase $\Delta\varphi$ of pulses and photoelectron kinetic energies. Upper row: Angular and relative phase $\Delta\varphi$-dependent photoelectron spectra at energies (a) 0.67 eV, peak 2, (b) 0.97 eV, peak 3, and (c) 1.25 eV, peak 4. For comparison, we also plot the corresponding intensity of spectra for different angles (d) $0° \pm 20°$ (angle I) and (e) $45° \pm 15°$ (angle II) for the three peaks 2, 3, and 4 in Fig. 2(a). (f) The maxima in (d) and (e) vs the relative phase $\Delta\varphi$.

Gaussian envelope $f(t)$ to average over the pulse frequencies as (see Supplemental Material [40])

$$P_{\text{int}}(\varepsilon_k) = \left(\alpha_0 + \alpha_1 e^{-\alpha_2 \Delta \varepsilon_k^2}\right) \cos(\theta - \Delta \varphi). \qquad (7)$$

α_i $(i = 0, 1, 2)$ are coefficients which are determined by the pulse duration and intensity.

From Eq. (7) we see that the interference term $P_{\text{int}}(\varepsilon_k)$ of the photoelectron angular distributions initiated from the combined electronic states is composed of two components: (i) the interference between the direct A and B three-photon (3ω) and two-photon $(2\omega + \omega)$ transitions, $\alpha_0 \cos(\theta - \Delta \varphi)$, independent of electron energy, and (ii) the interference between the two $A\,^2\Sigma^+$ and $B\,^2\Pi$ electronic states, $\alpha_1 e^{-\alpha_2 \Delta \varepsilon_k^2} \cos(\theta - \Delta \varphi)$]. For both cases, the evolution of the photoelectron angular distributions is a function of the relative phase $\theta - \Delta \varphi$. Due to the effects of the electronic coherent interference, as predicted in Eq. (7), the interference is modified by the energy differences $\Delta \varepsilon_k$, with a function of $e^{-\alpha_2 \Delta \varepsilon_k^2}$. The variation of $\Delta \varepsilon_k$ produces a modulation of the multiple pathway ionization interference. As a result, increasing the photoelectron kinetic energy leads to a shift of the maxima of the phase-dependent interference patterns, as illustrated in Fig. 3. Therefore, photoelectron spectra at various photoelectron energies ε and emission angles show different dependences on the relative phase $\Delta \varphi$ of pulses, as predicted in Eq. (7).

In summary, we have experimentally presented a scheme to explore coherent interference between electronic states in molecules by ultrafast two-color phase-controlled femtosecond laser pulses. A coherent superposition is created between two excited electronic states with different symmetries, which are simultaneously ionized. In spite of the nonorientation of NO molecules, the photoelectron occurs mainly at particular angles due to the orbital symmetry. With the assistance of coherent control pulses, multiple pathway ionization leads to asymmetric interference patterns in photoelectron angular distributions of NO which are shown to be dependent on the relative phase $\Delta \varphi$ of the pulses and their effects on ionization from orbitals of different symmetries. It is also found that the phase dependence is sensitive to the photoelectron energy, involving the dynamics of the coherent-state interference. Numerical simulations of molecular TDSEs and theoretical analysis confirm the experimental demonstrations and have shown that such electronic state coherence can be measured from photoelectron interference patterns in diatomics produced by phase-controlled two-color laser pulses. Our findings demonstrate that the modification of the multiple pathway ionization interference in the photoelectron kinetic energy spectra is a fingerprint of the ultrafast coherent dynamics of electronic states. The results pave the way to control and image coherent electron dynamics in molecules by ultrashort laser pulses which can be extended to other complex molecules, and therefore demonstrate a great potential for exploring intramolecular coherent electronic dynamics in molecular reactions without necessary preorientation [46,47].

---

[1] A. H. Zewail, J. Phys. Chem. A **104**, 5660 (2000).

[2] D. Shorokhov and A. H. Zewail, J. Chem. Phys. **144**, 080901 (2016).

[3] J. H. Baraban, P. B. Changala, G. Ch. Mellau, J. F. Stanton, A. J. Merer, and R. W. Field, Science **350**, 1338 (2015).

[4] H. C. Shao and A. F. Starace, Phys. Rev. Lett. **105**, 263201 (2010).

[5] S. Chelkowski, P. B. Corkum, and A. D. Bandrauk, Phys. Rev. Lett. **82**, 3416 (1999).

[6] B. Erk, R. Boll, S. Trippel, D. Anielski, L. Foucar, B. Rudek, S. W. Epp, R. Coffee, S. Carron, S. Schorb, K. R. Ferguson, M. Swiggers, J. D. Bozek, M. Simon, T. Marchenko, J. Küpper, I. Schlichting, J. Ullrich, C. Bostedt, D. Rolles, and A. Rudenko, Science **345**, 288 (2014).

[7] M. Meckel, D. Comtois, D. Zeidler, A. Staudte, D. Pavičić, H. C. Bandulet, H. Pépin, J. C. Kieffer, R. Dörner, D. M. Villeneuve, and P. B. Corkum, Science **320**, 1478 (2008).

[8] C. I. Blaga, J. Xu, A. D. DiChiara, E. Sistrunk, K. Zhang, P. Agostini, T. A. Miller, L. F. DiMauro, and C. D. Lin, Nature (London) **483**, 194 (2012).

[9] B. Wolter, M. G. Pullen, A.-T. Le, M. Baudisch, K. Doblhoff-Dier, A. Senftleben, M. Hemmer, C. D. Schröter, J. Ullrich, T. Pfeifer, R. Moshammer, S. Gräfe, O. Vendrell, C. D. Lin, and J. Biegert, Science **354**, 308 (2016).

[10] Y. Ito, C. Wang, A.-T. Le, M. Okunishi, D. Ding, C. D. Lin, and K. Ueda, Struct. Dynam. **3**, 034303 (2016).

[11] K. J. Yuan, C. C. Shu, D. Dong, and A. D. Bandrauk, J. Phys. Chem. Lett. **8**, 2229 (2017).

[12] D. M. Villeneuve, P. Hockett, M. J. J. Vrakking, and H. Niikura, Science **356**, 1150 (2017).

[13] E. Goulielmakis, Z.-H. Loh, A. Wirth, R. Santra, M. Rohringer, V. S. Yakovlev, S. Zherebtsov, T. Pfeifer, A. M. Azzeer, M. F. Kling, S. R. Leone, and F. Krausz, Nature (London) **466**, 739 (2010).

[14] K. J. Yuan and A. D. Bandrauk, Phys. Chem. Chem. Phys. **19**, 25846 (2017).

[15] P. M. Kraus, B. Mignolet, D. Baykusheva, A. Rupenyan, L. Horný, E. F. Penka, G. Grassi, O. I. Tolstikhin, J. Schneider, F. Jensen, L. B. Madsen, A. D. Bandrauk, F. Remacle, and H. J. Wörner, Science **350**, 790 (2015).

[16] A. S. Alnaser, M. Kübel, R. Siemering, B. Bergues, Nora G Kling, K. J. Betsch, Y. Deng, J. Schmidt, Z. A. Alahmed, A. M. Azzeer, J. Ullrich, I. Ben-Itzhak, R. Moshammer, U. Kleineberg, F. Krausz, R. de Vivie-Riedle, and M. F. Kling, Nat. Commun. **5**, 3800 (2014).

[17] M. R. Miller, Y. Xia, A. Becker, and A. Jaroń-Becker, Optica **3**, 259 (2016).

[18] A. García-Vela and N. E. Henriksen, J. Phys. Chem. Lett. **6**, 824 (2015).

[19] K. L. Reid, D. J. Leahy, and R. N. Zare, J. Chem. Phys. **95**, 1746 (1991).

[20] A. Sen, S. T. Pratt, and K. L. Reid, J. Chem. Phys. **147**, 013927 (2017).

[21] R. B. López-Martens, T. W. Schmidt, and G. Roberts, Phys. Rev. A **62**, 013414 (2000).

[22] T. Dove, T. W. Schmidt, R. B. López-Martens, and G. Roberts, Chem. Phys. **267**, 115 (2001).

[23] Z. G. Sun, H. P. Liu, N. Q. Lou, and S. L. Cong, Chem. Phys. Lett. **369**, 374 (2003).

[24] Q. T. Meng, G. H. Yang, H. L. Sun, K. L. Han, and N. Q. Lou, Phys. Rev. A **67**, 063202 (2003).

[25] S. M. Wang, S. L. Cong, K. J. Yuan, and Y. Y. Niu, Chem. Phys. Lett. **417**, 164 (2006).

[26] B. Wang, B. Liu, Y. Wang, and L. Wang, Phys. Rev. A **81**, 043421 (2010).

[27] A. T. J. B. Eppink and D. H. Parker, Rev. Sci. Instrum. **68**, 3477 (1997).

[28] J. Yu, W. Hu, X. Li, P. Ma, L. He, F. Liu, C. Wang, S. Luo, and D. Ding, J. Phys. B **50**, 235602 (2017).

[29] M. J. J. Vrakking, Rev. Sci. Instrum. **72**, 4084 (2001).

[30] J. P. Farrell, S. Petretti, J. Förster, B. K. McFarland, L. S. Spector, Y. V. Vanne, P. Decleva, P. H. Bucksbaum, A. Saenz, and M. Gühr, Phys. Rev. Lett. **107**, 083001 (2011).

[31] F. R. Gillmorre, J. Quantum Spectrosc. Radiat. Transfer **5**, 369 (1965).

[32] T. Bredtmann, S. Chelkowski, and A. D. Bandrauk, Phys. Rev. A **84**, 021401 (2011).

[33] A. Gijsbertsen, W. Siu, M. F. Kling, P. Johnsson, P. Jansen, S. Stolte, and M. J. J. Vrakking, Phys. Rev. Lett. **99**, 213003 (2007).

[34] A. Staudte, D. Pavičić, S. Chelkowski, D. Zeidler, M. Meckel, H. Niikura, M. Schöffler, S. Schössler, B. Ulrich, P. P. Rajeev, Th. Weber, T. Jahnke, D. M. Villeneuve, A. D. Bandrauk, C. L. Cocke, P. B. Corkum, and R. Dörner, Phys. Rev. Lett. **98**, 073003 (2007).

[35] X. Gong, P. He, Q. Song, Q. Ji, H. Pan, J. Ding, F. He, H. Zeng, and J. Wu, Phys. Rev. Lett. **113**, 203001 (2014).

[36] Z. Bacic and J. C. Light, Annu. Rev. Phys. Chem. **40**, 469 (1989).

[37] Z. Sun and N. Lou, Phys. Rev. Lett. **91**, 023002 (2003).

[38] A. L'Huillier, L. A. Lompré, D. Normand, X. Tang, and P. Lambropoulos, J. Opt. Soc. Am. B **6**, 1790 (1989).

[39] F. Fillion-Gourdeau, E. Lorin, and A. D. Bandrauk, J. Phys. A **45**, 215304 (2012).

[40] See Supplemental Material at http://link.aps.org/supplemental/10.1103/PhysRevA.99.011402 for an interference model of coherent electronic states by two-color laser pulses.

[41] J. Wu, L. Ph. H. Schmidt, M. Kunitski, M. Meckel, S. Voss, H. Sann, H. Kim, T. Jahnke, A. Czasch, and R. Dörner, Phys. Rev. Lett. **108**, 183001 (2012).

[42] G. Lagmago Kamta and A. D. Bandrauk, Phys. Rev. A **74**, 033415 (2006).

[43] H. L. Kim and R. Bersohn, J. Chem. Phys. **107**, 4546 (1997).

[44] J. M. Ngoko Djiokap, S. X. Hu, L. B. Madsen, N. L. Manakov, A. V. Meremianin, and A. F. Starace, Phys. Rev. Lett. **115**, 113004 (2015).

[45] K. J. Yuan, S. Chelkowski, and A. D. Bandrauk, Phys. Rev. A **93**, 053425 (2016).

[46] A. Comby, S. Beaulieu, M. Boggio-Pasqua, D. Descamps, F. Légaré, L. Nahon, S. Petit, B. Pons, B. Fabre, Y. Mairesse, and V. Blanchet, J. Phys. Chem. Lett. **7**, 4514 (2016).

[47] S. Beaulieu, A. Comby, D. Descamps, B. Fabre, G. A. Garcia, R. Géneaux, A. G. Harvey, F. Légaré, Z. Mašín, L. Nahon, A. F. Ordonez, S. Petit, B. Pons, Y. Mairesse, O. Smirnova, and V. Blanchet, Nat. Phys. **14**, 484 (2018)